Hindawi
Scientific Programming
Volume 2020, Article ID 6348372, 18 pages
https://doi.org/10.1155/2020/6348372

Research Article

Isomap-Based Three-Dimensional Operational Modal Analysis

Cheng Wang,[1,2] **Weihua Fu**,[1] **Haiyang Huang**,[1] **and Jianwei Chen**[3]

[1]*College of Computer Science and Technology, Huaqiao University, Xiamen 361021, China*
[2]*State Key Laboratory for Strength and Vibration of Mechanical Structures, Xi'an Jiaotong University, Xi'an 710049, China*
[3]*Department of Mathematics and Statistics, San Diego State University, San Diego, CA 92182, USA*

Correspondence should be addressed to Cheng Wang; wangcheng@hqu.edu.cn

Received 7 February 2020; Revised 2 June 2020; Accepted 9 June 2020; Published 14 July 2020

Academic Editor: Chenxi Huang

In order to identify the modal parameters of time invariant three-dimensional engineering structures with damping and small nonlinearity, a novel isometric feature mapping (Isomap)-based three-dimensional operational modal analysis (OMA) method is proposed to extract nonlinear features in this paper. Using this Isomap-based OMA method, a low-dimensional embedding matrix is multiplied by a transformation matrix to obtain the original matrix. We find correspondence relationships between the low-dimensional embedding matrix and the modal coordinate response and between the transformation matrix and the modal shapes. From the low-dimensional embedding matrix, the natural frequencies can be determined using a Fourier transform and the damping ratios can be identified by the random decrement technique or natural excitation technique. The modal shapes can be estimated from the Moore–Penrose matrix inverse of the low-dimensional embedding matrix. We also discuss the effects of different parameters (i.e., number of neighbors and matrix assembly) on the results of modal parameter identification. The modal identification results from numerical simulations of the vibration response signals of a cylindrical shell under white noise excitation demonstrate that the proposed method can identify the modal shapes, natural frequencies, and ratios of three-dimensional structures in operational conditions only from the vibration response signals.

1. Introduction

Operational modal analysis (OMA) has received widespread attention because it enables the identification of the modal parameters of a structure in its working condition using only the vibration response [1]. Modal parameters (including the modal natural frequencies, modal shapes, and modal damping ratios) are essential for structural vibration control, damage diagnosis, and so on [2, 3]. Recently, blind source separation (BSS) methods such as sparse component analysis (SCA) [4, 5] and independent component analysis (ICA) [6] have been widely used for output-only identification.

Dimensionality reduction techniques are an effective means of overcoming the curse of dimensionality. Current methods can be categorized as either linear or nonlinear dimensionality reduction [7]. Classical linear dimensionality reduction algorithms include principal component analysis (PCA) [8], locality preserving projection (LPP) [9], multidimensional scaling (MDS) [10], and linear discriminant analysis (LDA) [11]. Recently, Wang et al. introduced PCA to OMA [12] and proposed PCA and second-order blind identification- (SOB-I-) based three-dimensional OMA methods [13, 14]. However, the time invariant engineering structures are often three-dimensional, with damping and small nonlinearity [15].

Similarly, there are many nonlinear dimensionality reduction methods, such as locally linear embedding (LLE) [16, 17], Laplacian eigenmaps (LE) [18], kernel PCA [19], and isometric feature mapping (Isomap) [20]. Bai et al. proposed an LLE-based OMA method for three-dimensional structures [21], Zhang et al. optimized the nearest neighbor selection method for LLE-based OMA [22], Dong et al. introduced modal identification and influence factors of LLE algorithm [23], and Guan et al. made comprehensive and systematic comparisons of four statistical learning algorithms (PCA, ICA, SOBI, and LLE) on analyzing their performance for resolving operational modal parameters identification [24]. This paper applies Isomap to OMA.

Isomap is a nonlinear dimensionality reduction algorithm for manifold learning [25]. This method can find meaningful low-dimensional structures hidden in their high-dimensional observations. This idea can be used in OMA. To date, Isomap has been widely used in various fields [26].

Based on Isomap algorithm, this paper proposes a three-dimensional OMA method for complex three-dimensional continuum structures.

The primary contributions of this paper can be summarized as follows:

(1) An Isomap-based OMA method is proposed for the identification of modal shapes, modal natural frequencies, and modal ratios of three-dimensional structures

(2) We identify the correspondence between the low-dimensional embedding matrix and the modal response matrix and between the transformation matrix and the modal shapes

(3) We conduct a theoretical analysis of the characteristics of the Isomap-based OMA method

(4) We analyze the effects of different parameters (e.g., matrix assembly method, number of neighbors, and dimensionality reduction method) on the algorithm

(5) We design numerical simulations of the vibration response signals of a cylindrical shell to verify the effectiveness of our algorithm

The remainder of this paper is organized as follows. In Section 2, the Isomap-based OMA method for three-dimensional modal parameter identification and the characteristics of the proposed method are introduced. The effect of various parameters is investigated in Section 3. Section 4 presents the simulation verification results. Finally, we conclude the paper in Section 5.

2. Isomap-Based Three-Dimensional Operational Modal Analysis

2.1. Stationary Response Signals Decomposition in Modal Coordinate and Operational Modal Identification. According to dynamic structural vibration theory, the dynamic differential equation of a d-degree-of-freedom (DOF) linear system in the physical coordinate system is

$$\mathbf{M}\ddot{\mathbf{X}}(t) + \mathbf{C}\dot{\mathbf{X}}(t) + \mathbf{K}\mathbf{X}(t) = \mathbf{F}(t), \tag{1}$$

where $\mathbf{M} \in \mathbb{R}^{D\times D}$ is the mass matrix, $\mathbf{C} \in \mathbb{R}^{D\times D}$ is the damping matrix, $\mathbf{K} \in \mathbb{R}^{D\times D}$ is the stiffness matrix, $F(t) \in \mathbb{R}^{D\times T}$ is the external excitation, and $\ddot{\mathbf{X}}(t), \dot{\mathbf{X}}(t), \mathbf{X}(t) \in \mathbb{R}^{D\times T}$ are the acceleration, speed, and displacement response signals, respectively.

The free and random vibrations of weakly damped systems have a displacement response that can be expressed as follows in modal coordinates:

$$\mathbf{X}(t) \approx \mathbf{\Phi}\mathbf{Q}(t) = \sum_{i=1}^{d} \vec{\phi}_i \vec{q}_i(t), \tag{2}$$

where $\mathbf{\Phi} \in \mathbb{R}^{D\times d}$ is the modal shapes matrix constituted by the modal shape $\vec{\phi}_i$ of each order and $\mathbf{Q}(t) \in \mathbb{R}^{d\times T}$ is the modal response matrix formed by the modal responses $\vec{q}_i(t)$. When the order of each natural frequency is different, the modal shape vector $\vec{\phi}_i \in \mathbb{R}^{d\times 1}$ becomes

$$\begin{aligned} \mathbf{\Phi}^T\mathbf{M}\mathbf{\Phi} &= \mathbf{M} = \operatorname{diag}\left[\vec{m}_1, \vec{m}_2, \ldots, \vec{m}_i \ldots, \vec{m}_d\right], \\ \mathbf{\Phi}^T\mathbf{K}\mathbf{\Phi} &= \mathbf{K} = \operatorname{diag}\left[\vec{k}_1, \vec{k}_2, \ldots, \vec{k}_i \ldots, \vec{k}_d\right]. \end{aligned} \tag{3}$$

The modal responses $\vec{q}_i(t)$ are independent of each other and $\Lambda_{d\times d}$ is a diagonal matrix:

$$E\left[\mathbf{Q}(t)\mathbf{Q}^T(t)\right] = \mathbf{\Lambda}_{d\times d}. \tag{4}$$

Taking advantage of single-DOF (SDOF) identification approach such as FFT, it is easy to recognize the ith natural frequency and modal damping ratio from the modal responses $\vec{q}_i(t)$.

After $\mathbf{Q}(t)$ has been obtained, the modal shape matrix Φ can be estimated using the Moore–Penrose matrix inverse:

$$\mathbf{\Phi} = \mathbf{X}(t)\mathbf{Q}^T(t)\left(\mathbf{Q}(t)\mathbf{Q}^T(t)\right)^{-1}. \tag{5}$$

OMA is to identify modal shape matrix Φ, natural frequencies, and modal damping ratios only from the vibration response signals $\mathbf{X}(t)$.

2.2. Isomap-Based OMA. Isomap is a very popular manifold learning algorithm. Unlike PCA, which is designed only for linear dimensionality reduction, Isomap can solve nonlinear dimensionality reduction problems [27]. The dimension-reducing Isomap algorithm takes the sample set $\mathbf{X}(t) = \{\vec{x}_1, \vec{x}_2, \ldots, \vec{x}_T\} \in \mathbb{R}^{D\times T}$ as input, where D is the number of dimensions and T is the number of samples. The values of two hyperparameters are then set: the number of neighbors K and the low-dimensional space dimension d. The output of the algorithm is the matrix of samples in low-dimensional space $\mathbf{S}(t) = \{\vec{s}_1, \vec{s}_2, \ldots, \vec{s}_T\} \in \mathbb{R}^{d\times T}$. The steps involved in the algorithm can be described as follows:

(1) Build a neighborhood graph G. For each sample point $x_{ij} \in \vec{x}_i \in \mathbb{R}^{D\times 1}, 1 \le i \le T,\ 1 \le j \le D$, we first calculate which points are its neighbors. Based on the Euclidean distance, all points within some fixed radius ε or the K nearest neighbors are selected. The points between x_{ij} and its neighbors are then connected, as shown in Figure 1. These neighborhood relations are represented as a weighted graph G over the data points.

(2) Estimate the geodesic distances. Call the shortest path algorithm to calculate the distance between any two points. This is also called the geodesic distance, that is, the distance to the adjacent point is the Euclidean distance, and that to the nonadjacent point is the shortest path distance. The specific calculation process for the distance matrix $\mathbf{B}(t) \in \mathbb{R}^{T\times T}$ is given in (6)–(10).

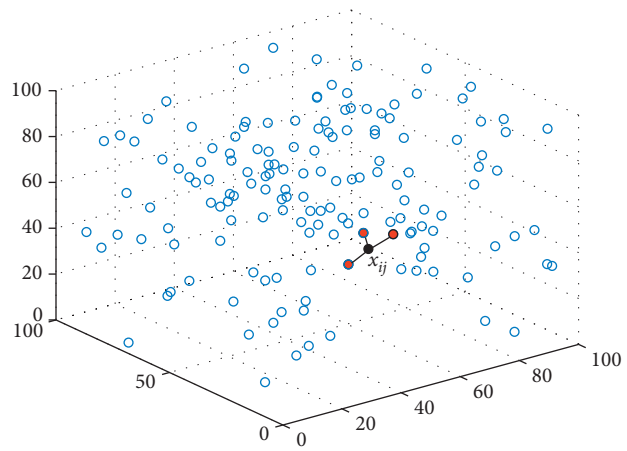

Figure 1: Connection of a sample to its neighbors in the Isomap algorithm.

(3) Call the classical multidimensional scaling (MDS) algorithm to obtain the matrix $\mathbf{S}(t)$ of the sample set in the low-dimensional space.

The following can be obtained from the steps of MDS. The aim of the MDS algorithm is to obtain the representation of the sample in the d-dimensional space, $\mathbf{S}(t) = \{\vec{s}_1, \vec{s}_2, \ldots, \vec{s}_T\} \in \mathbb{R}^{D\times T}, d < D$. The geodesic distance of any two samples in the d-dimensional space is equal to the distance in the original space, which means $\|s_i - \vec{s}_j\| = \text{dist}_{ij}$ and dist_{ij} is the distance between any two samples.

Setting $\mathbf{B}(t) = \mathbf{S}(t)^T\mathbf{S}(t) \in \mathbb{R}^{T\times T}$, we have that $b_{ij} = \vec{s}_i^T\vec{s}_j$, so the following equation can be obtained:

$$d_{ij}^2 = \left\|\vec{s}_i - \vec{s}_j\right\|^2 = \left\|\vec{s}_i\right\|^2 + \left\|\vec{s}_j\right\|^2 - 2\vec{s}_i^T\vec{s}_j = b_{ii} + b_{jj} - 2b_{ij}. \tag{6}$$

From the following equations

$$\text{dist}_{i\cdot}^2 = \frac{1}{T}\sum_{j=1}^{T} d_{ij}^2, \tag{7}$$

$$\text{dist}_{\cdot j}^2 = \frac{1}{T}\sum_{i=1}^{T} d_{ij}^2, \tag{8}$$

$$\text{dist}_{\cdot\cdot}^2 = \frac{1}{T^2}\sum_{i=1}^{T}\sum_{j=1}^{T} d_{ij}^2, \tag{9}$$

we obtain that

$$b_{i,j} = \frac{d_{i,\cdot}^2 + d_{\cdot,j}^2 - d_{\cdot,\cdot}^2 - d_{ij}^2}{2}. \tag{10}$$

In summary, the classical MDS algorithm can be split into the following steps:

(1) Using (7)–(9), calculate $\text{dist}_{i\cdot}^2$, $\text{dist}_{\cdot j}^2$, and $\text{dist}_{\cdot\cdot}^2$

(2) Using (10), compute the matrix $\mathbf{B}(t)$

(3) Perform eigenvalue decomposition on $\mathbf{B}(t)$

(4) Construct $\widetilde{\mathbf{\Lambda}}$ as the diagonal matrix of the d largest eigenvalues and $\widetilde{\mathbf{V}}$ as the corresponding eigenvector matrix

(5) $\mathbf{S}(t) = \widetilde{\mathbf{V}}\widetilde{\mathbf{\Lambda}}^{1/2} \in \mathbb{R}^{T\times d}$ contains the low-dimensional coordinates for each sample

We now introduce the Isomap algorithm; an example of using Isomap for nonlinear dimensionality reduction is presented in Figure 2 [25]. (a) of Figure 2 is a dataset of three-dimensional space. After the dimensionality reduction by Isomap algorithm, the dataset of two-dimensional space (Figure 2(b)) still maintains the internal connection of three-dimensional space data.

PCA and classical MDS can be effectively applied to Euclidean structures but fail to extract nonlinear features [21]. The Isomap algorithm is an improved version of the classical MDS method that can solve nonlinear problems. More specifically, the dimensionality reduction principle of the Isomap method makes the Euclidean distance between the low-dimensional data equal to the geodesic distance between the high-dimensional data. When calculating the distance between data points on a high-dimensional manifold, instead of applying the traditional Euclidean distance, Isomap uses the geodesic distance in the differential geometry and estimates this distance using actual input data.

The Isomap algorithm can obtain low-dimensional representations $\mathbf{S}(t) \in \mathbb{R}^{d\times T}$ that are also independent, so there exists

$$\mathbf{H} = \mathbf{X}(t)\mathbf{S}^T(t)\left(\mathbf{S}(t)\mathbf{S}^T(t)\right)^{-1}, \tag{11}$$

where $\mathbf{H}$ is the transformation matrix. Therefore, $\mathbf{X}(t)$ has the following form:

$$\mathbf{X}(t) \approx \mathbf{H}\mathbf{S}(t) = \sum_{j=1}^{d} \vec{h}_j\vec{s}_j(t). \tag{12}$$

Comparing (2) and (12), we can conclude that there is a one-to-one corresponding mapping relationship between the modal shape matrix Φ in modal coordinate and transformation matrix $\mathbf{H}$ in Isomap, the modal responses matrix $\mathbf{Q}(t)$ in modal coordinate, and low-dimensional representations $\mathbf{S}(t)$ in Isomap. Figure 3 shows a physical interpretation of Isomap-based OMA.

2.3. Three-Dimensional Modal Parameter Identification. The OMA of "three-dimensional" structure is a more complex problem, because it requires the assembly of the modal parameter in three directions to calculate the "three-dimensional" modal parameter.

Therefore, we introduce two three-dimensional matrix assembly methods in this section, namely, least-squares matrix substitution (LSMS) and direct matrix assembly (DMA). After the data matrix has been assembled, we use the Isomap algorithm to find the modal parameters.

Continuum-structure mechanical systems can be divided into D discrete observation components at regular intervals. The displacement response of a three-dimensional cylindrical shell in the time domain can be expressed by its

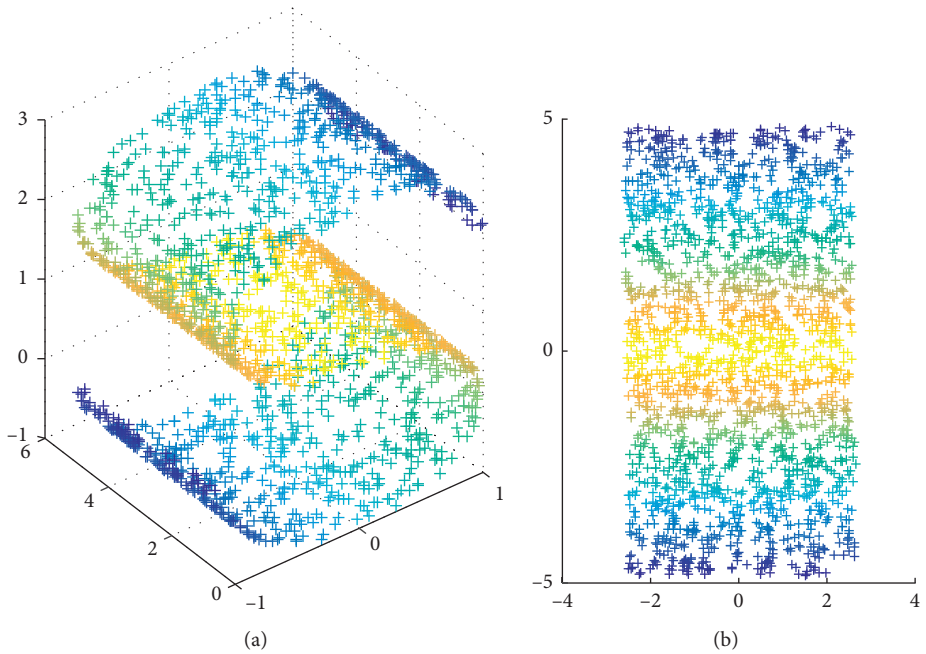

Figure 2: An example of using Isomap for nonlinear dimensionality reduction: (a) original three-dimension data before dimensionality reduction; (b) two-dimension data after dimensionality reduction by Isomap.

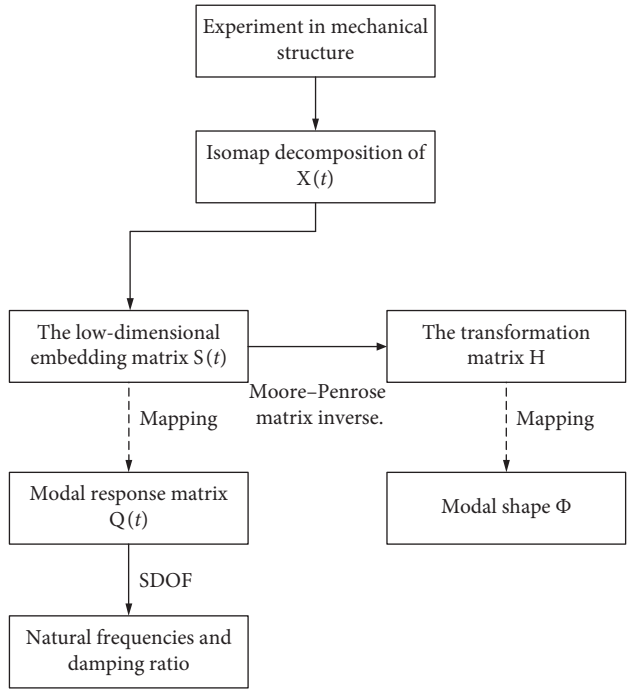

Figure 3: Physical interpretation of Isomap-based OMA.

modal coordinate approximation when D is sufficiently large:

$$\begin{cases} \mathbf{X}(t) = \mathbf{U}\mathbf{Q}(t) = \sum_{i=1}^{d} \vec{u}_i \vec{q}_i(t), \\ \mathbf{Y}(t) = \mathbf{V}\mathbf{Q}(t) = \sum_{i=1}^{d} \vec{v}_i \vec{q}_i(t), \\ \mathbf{Z}(t) = \mathbf{W}\mathbf{Q}(t) = \sum_{i=1}^{d} \vec{w}_i \vec{q}_i(t). \end{cases} \tag{13}$$

In (13), $\mathbf{X}(t), \mathbf{Y}(t), \mathbf{Z}(t) \in \mathbb{R}^{D\times T}$ are the vibration responses in three directions, d is the embedding dimension, $\mathbf{U}$, $\mathbf{V}$, $\mathbf{W}$ are the modal shapes in three directions, T is the sampling time, and the modal response matrix $\mathbf{Q}(t)$ of each dimension is the same. Using the minimum square sum of errors as the objective function to be optimized, the Moore–Penrose matrix inverse of (13) is [13]

$$\begin{cases} \mathbf{U} = \mathbf{X}(t)\mathbf{Q}^T(t)\left[\mathbf{Q}(t)\mathbf{Q}^T(t)\right]^{-1}, \\ \mathbf{V} = \mathbf{Y}(t)\mathbf{Q}^T(t)\left[\mathbf{Q}(t)\mathbf{Q}^T(t)\right]^{-1}, \\ \mathbf{W} = \mathbf{Z}(t)\mathbf{Q}^T(t)\left[\mathbf{Q}(t)\mathbf{Q}^T(t)\right]^{-1}. \end{cases} \tag{14}$$

In the LSMS-based Isomap method, a single-dimensional displacement response signal is first decomposed. To reduce the influence of the Gaussian-distributed signal measurement noise, the main and biggest structure's dynamic response dimension is selected in practical engineering cases. Substituting $\mathbf{Q}(t)$ into the other two-dimensional displacement response signals using the Moore–Penrose matrix inverse in (14), the modal shapes of these two dimensions can be identified. Three-dimensional modal shapes $[\vec{u}_i, \vec{v}_i, \vec{w}_i]\, i = 1, 2, \ldots, d$ are then assembled. To identify the operational modal parameters of the three-dimensional structure, the following strategy is adopted and the process of identification is performed for the three-dimensional structure. The process is described in Figure 4, where it is assumed that the vibration response is greatest in the $\mathbf{X}(t)$ direction.

From (13), we know that the modal response matrix $\mathbf{Q}(t)$ of each dimension is the same. Therefore, the DMA method assembles the modal response in three directions as the overall modal response $\mathbf{A}(t) \in \mathbb{R}^{3D\times T}$ of the entire structure [28]:

$$\mathbf{A}(t) = \begin{bmatrix} \mathbf{X}(t) \\ \mathbf{Y}(t) \\ \mathbf{Z}(t) \end{bmatrix}. \tag{15}$$

The modal coordinate response and modal shape of the overall structure are solved in one pass:

$$\mathbf{A}(t) = \begin{bmatrix} \mathbf{X}(t) \\ \mathbf{Y}(t) \\ \mathbf{Z}(t) \end{bmatrix} = \begin{bmatrix} \mathbf{U} \\ \mathbf{V} \\ \mathbf{W} \end{bmatrix} \mathbf{Q}(t). \tag{16}$$

Using the Moore–Penrose matrix inverse of (16), we can obtain the modal shapes of all three directions as

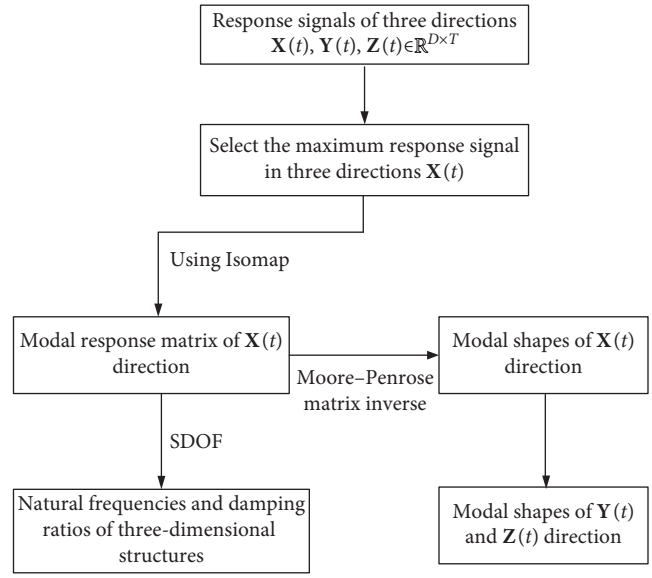

Figure 4: Process of LSMS-based Isomap for three-dimensional structure OMA.

$$\begin{bmatrix} \mathbf{U} \\ \mathbf{V} \\ \mathbf{W} \end{bmatrix} = \mathbf{A}(t)\mathbf{Q}^T(t)\left[\mathbf{Q}(t)\mathbf{Q}^T(t)\right]^{-1}. \tag{17}$$

The process of the DMA-based Isomap method for three-dimensional OMA is described in Figure 5.

2.4. Characteristics of Isomap-Based OMA. Isomap-based OMA has the following characteristics:

(1) The order of the identified modal parameters is different from the theoretical value. The Isomap algorithm is an improved version of classical MDS, and the order of recognition follows the contribution of the principal components, running from small to large.

(2) The amplitude information of the modal shapes is lost. According to (8), the modal shapes of each order are orthogonal to one another and the modal shape vector is unitized.

(3) Some modal information may be missing. When the contribution of an independent component is small, it is difficult to identify its modal parameters.

3. Effect of Parameters on the Algorithm

3.1. Matrix Assembly. The LSMS method selects the maximum vibration response data of the three-dimensional structure to calculate the modal response matrix, which is used to determine the other modal parameters. However, the modal coordinate response of the direction of maximum vibration response is not equal to the global modal coordinate response. Although we obtain this matrix at a small cost, the resulting three-dimensional modal shape must have a large error.

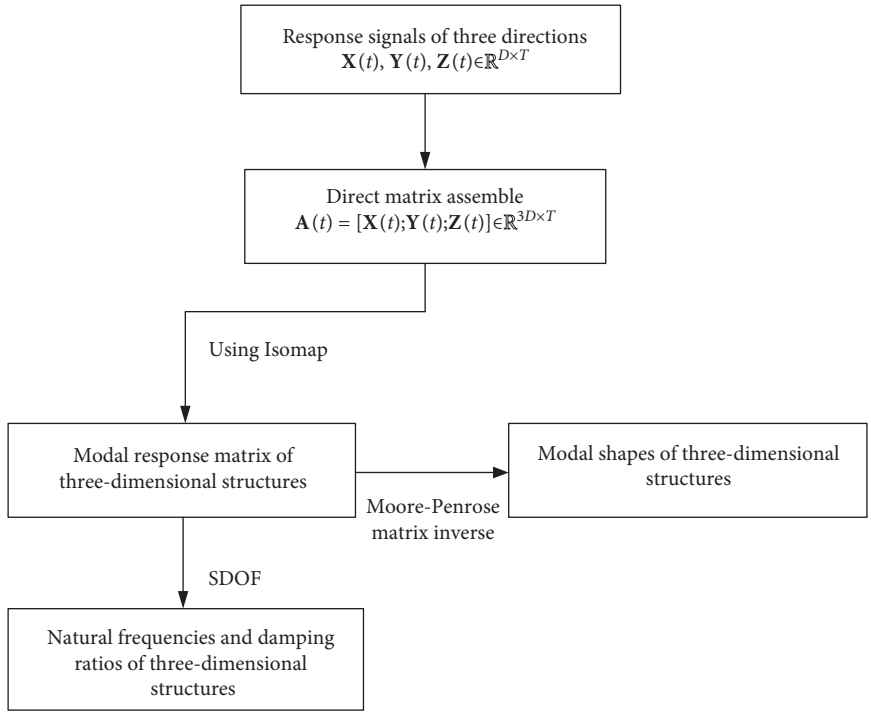

Figure 5: Process of DMA-based Isomap for three-dimensional structure OMA.

The DMA-based method directly obtains the global modal shape and overall modal coordinate response of three-dimensional structures and then uses Isomap to identify the modal parameters. Compared with LSMS, DMA avoids the need for matrix inversion operations and is more robust. Furthermore, this method offers greater accuracy because matrix inversion errors and ill-posed problems [29] are inevitable in the matrix decomposition calculation. Table 1 compares the performance of the two assembly methods [26].

Table 1: Performance comparison of two assembly methods in Isomap.

Matrix assembly methods	LSMS	DMA
Matrix inversion error	✓	×
Ill-posed problems	✓	×
Robustness	Sensitive to measurement noise	Insensitive to measurement noise

3.2. Number of Neighbors K. The neighbor value K refers to the number of data points to which a given point is connected. Each point is connected to the nearest K points to form a graph G, and then some algorithm (e.g., Dijkstra's algorithm and Floyd's algorithm) is used to calculate the shortest path.

If K is too small, the connectivity graph may not be formed, which will affect the calculation of the shortest distance. At the same time, the negative effects of noisy points will be amplified. A sufficiently large value of K can reduce the difference between the path length and the true geodesic distance. If K is too large, the computation time may become unbearable and underfitting may occur.

3.3. Linear and Nonlinear Methods. Both MDS and PCA are linear dimensionality reduction techniques. The PCA method looks for the low-dimensional embedding of the data points which best preserves their variance, as measured in the high-dimensional input space. The classical MDS method finds an embedding that preserves the interpoint distances. We use the Euclidean distance in the proposed method, and the results of PCA are consistent with those from MDS [21]. Our experimental results also confirm this.

Isomap is a nonlinear dimensionality reduction technique. When there are nonlinear features in the three-dimensional structures, the extraction performance of linear methods is poor. The linear and nonlinear relationships between the data also affect the algorithm results.

4. Simulation Verification and Result Analysis of Three-Dimensional Operational Modal Parameter Identification

4.1. Generation of Simulation Data. We conducted simulations to study a cylindrical shell with a complex three-dimensional structure. The cylindrical shell is simply supported at both ends, and a certain number of vibration sensors are positioned on its surface to record the vibration response in three directions, with a vibration exciter used to simulate the working conditions. Figure 6 illustrates this process.

The cylindrical shell has a thickness of 0.005 m, radius of 0.1825 m, length of 0.37 m, and elasticity modulus of

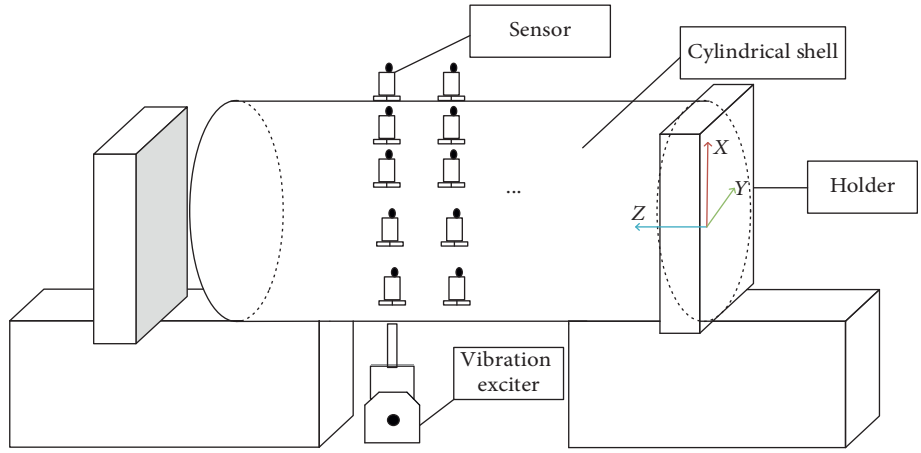

Figure 6: Simulation process.

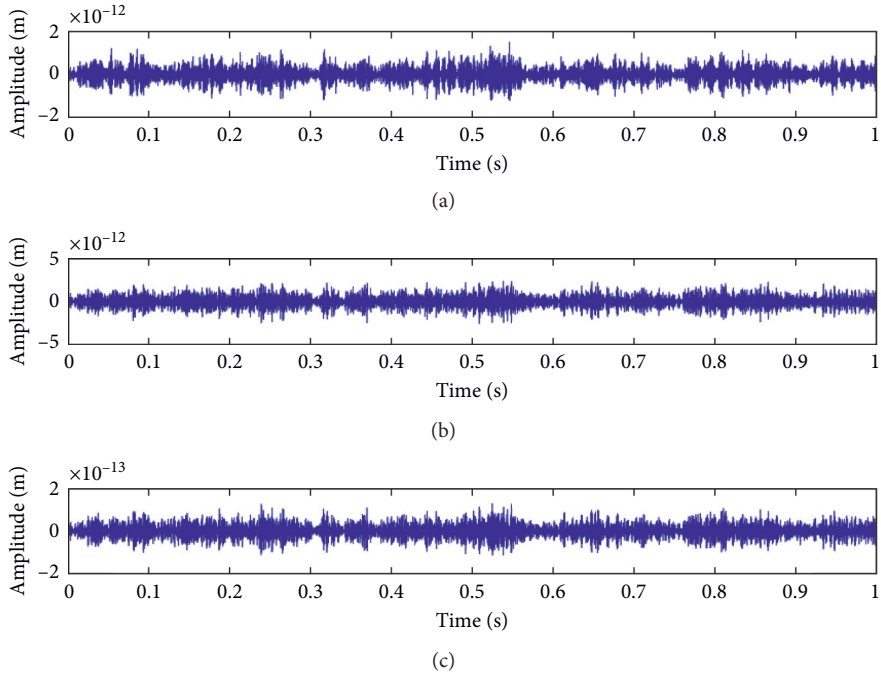

Figure 7: Response signals in three directions. (a) Response in X direction at the 1118th observation point. (b) Response in Y direction at the 1118th observation point. (c) Response in Z direction at the 1118th observation point.

205 GPa. The material has Poisson's ratio of 0.3, density of 7850 kg/m^3, and mode damping ratios of 0.03, 0.05, and 0.1.

The cylindrical shell was considered to be a uniform axial distribution of 38 circles, and each circle had 115 uniformly distributed observation points, giving a total of $D = 4370$ observation points. The sampling frequency was set to 5120 Hz, and the sampling time was set to 1 s. Finally, response signals in three directions were calculated by LMS Virtual Lab using finite element analysis (FEA). Response signals in the three directions at a random observation point are shown in Figure 7.

4.2. Evaluation Index. To evaluate the effect of identification using the proposed method for three-dimensional structures, the mode shapes and natural frequencies were calculated using FEA. These were considered the real modal parameters for comparison with the identified modal parameters. The modal assurance criterion (MAC) reflects the effectiveness of the modal identification given by the proposed method. MAC is defined as

$$\mathrm{MAC}_{\vec{\phi}_i, \vec{\varphi}_i} = \frac{\left(\vec{\phi}_i^{\,T} \vec{\varphi}_i\right)^2}{\left(\vec{\phi}_i^{\,T} \vec{\phi}_i\right)\left(\vec{\varphi}_i^{\,T} \vec{\varphi}_i\right)}, \tag{18}$$

where $\vec{\phi}_i$ is the identified ith-order modal shape and $\vec{\varphi}_i$ is the true ith-order modal shape. The MAC values range from 0 to 1, with higher values indicating a better correlation. The modals are all real, and there are no complexes.

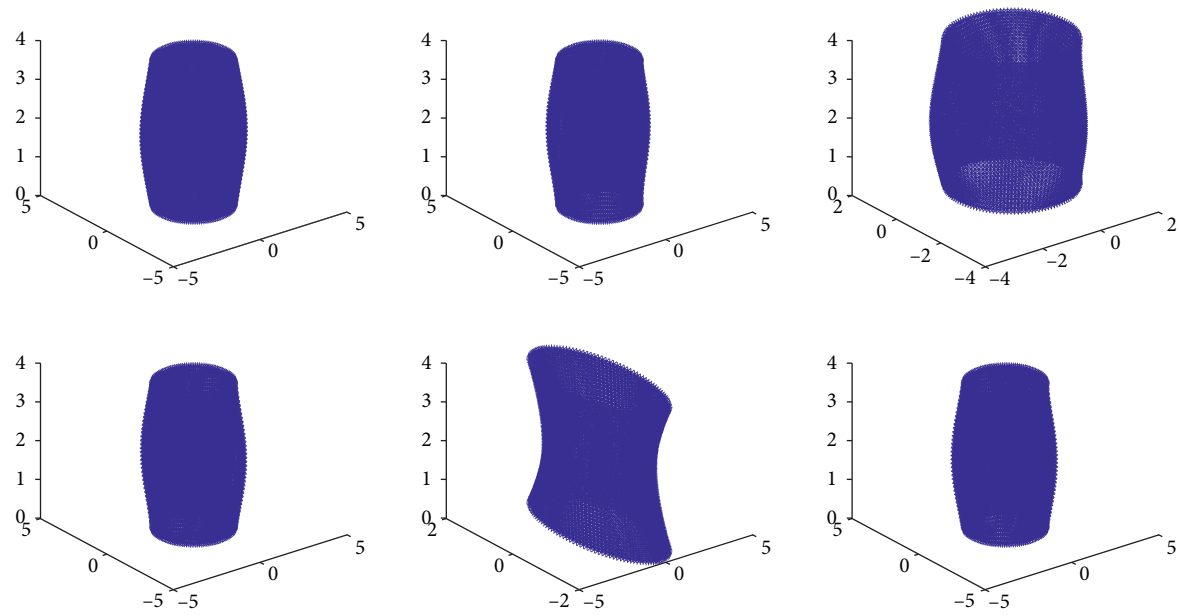

Figure 8: Real modal shapes calculated by FEA.

4.3. Simulation Results of Three-Dimensional Operational Modal Parameter Identification. From the response signals in the three directions shown in Figure 7, it is apparent that the vibration response in the $\mathbf{X}(t)$ direction is greater than those in the $\mathbf{Y}(t)$ and $\mathbf{Z}(t)$ directions. Thus, the LSMS-based method first used Isomap to decompose the $\mathbf{X}(t)$ direction.

The modal shapes and natural frequencies calculated by the FEA method with a damping ratio of 0.03 were considered to be the real values. Figure 8 shows the real modal shapes.

Embedding dimension of 6 and number of neighbors $K = 40$, when the modal response matrix $\mathbf{Q}(t)$ is obtained by Isomap, we apply a fast Fourier transform (FFT) to each of its columns and take the X-coordinate corresponding to the highest amplitude to be the modal natural frequencies of each order.

To enable a better comparison, we rotated the coordinates and obtained the results shown in Figure 9.

The modal shapes and natural frequencies identified by the LSMS-based Isomap algorithm are shown in Figures 10 and 11. Under the same conditions, the modal shapes and frequencies identified by the DMA-based Isomap algorithm are presented in Figures 12 and 13. Tables 2–5 compare the frequency, MAC of modal shapes, modal shapes, and modal ratios, respectively, identified by LSMS-based Isomap, DMA-based Isomap, and FEA.

The modal shape and frequency identified by the LSMS-based Isomap algorithm with an embedding dimension of 5 are shown in Figures 14 and 15.

Tables 6 and 7 compare the MAC and frequencies identified by the LSMS-based Isomap algorithm in different dimensions.

Tables 8–10 compare the MAC of modal shapes, modal frequencies, and modal damping ratios calculated by the LSMS and DMA methods for different numbers of neighbors K.

For the modal ratio, we apply the random decrement technique (RDT) [30] or natural excitation technique (NExT) [31] to each column of the modal response matrix $\mathbf{Q}(t)$ and then obtain the envelope of the curve from the Hilbert transform. Fitting an exponential decay to the envelope, the slope of best fit gives the modal ratio. Figure 16 illustrates this process.

We compare the modal damping ratio identification methods (RDT and NExT) using different dimensionality reduction methods (PCA [13]) in Tables 11–13. The results using LSMS to identify the MAC and frequencies are presented in Tables 14–16, and those using DMA are given in Tables 17–19.

4.4. Analysis of Simulation Results for Three-Dimensional Operational Modal Parameter Identification

(1) From Figures 8–13 and Tables 2–5, we can see that the DMA- and LSMS-based Isomap methods can effectively identify the modal shapes and frequencies. The DMA method does well in latter orders, whereas the LSMS method can better identify the first few orders of modal shapes. For the modal ratios, the DMA assembly method is better able to obtain the 6th-order results.

(2) From Tables 2–5, it can be concluded that the modal shapes and frequencies do not have a one-to-one correspondence. This is because the order of the mode coordinate vector is uncertain.

(3) From Figures 14 and 15 and Tables 6 and 7, the results of the five-dimensional case are the same as those of the first five dimensions of the six-

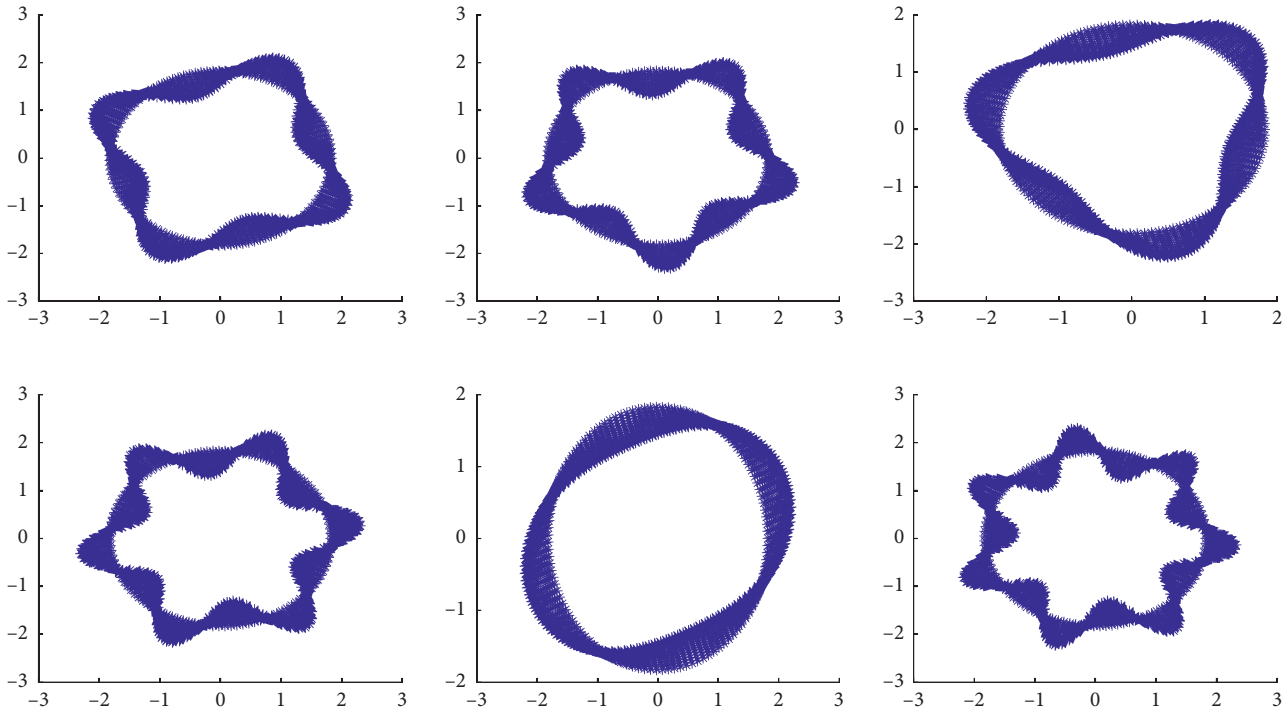

Figure 9: Real modal shapes after rotating the coordinates.

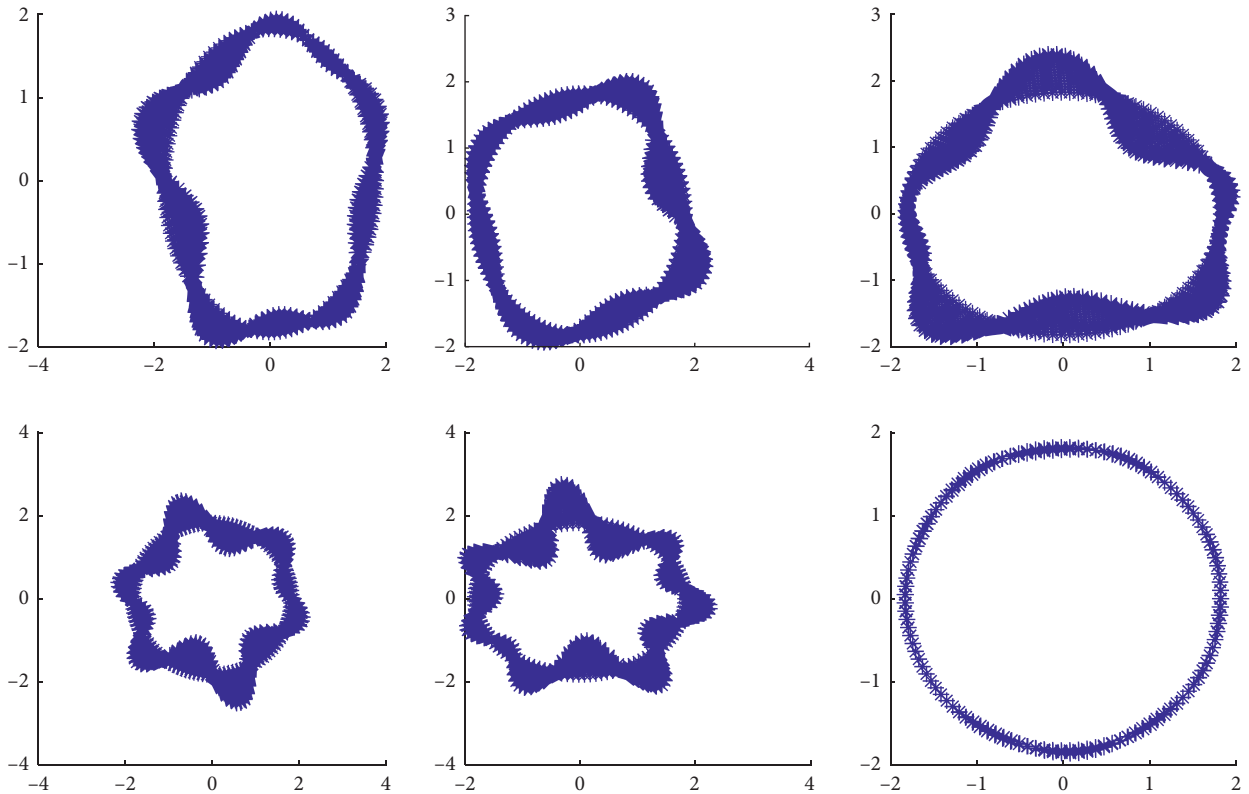

Figure 10: Modal shapes identified by LSMS-based Isomap.

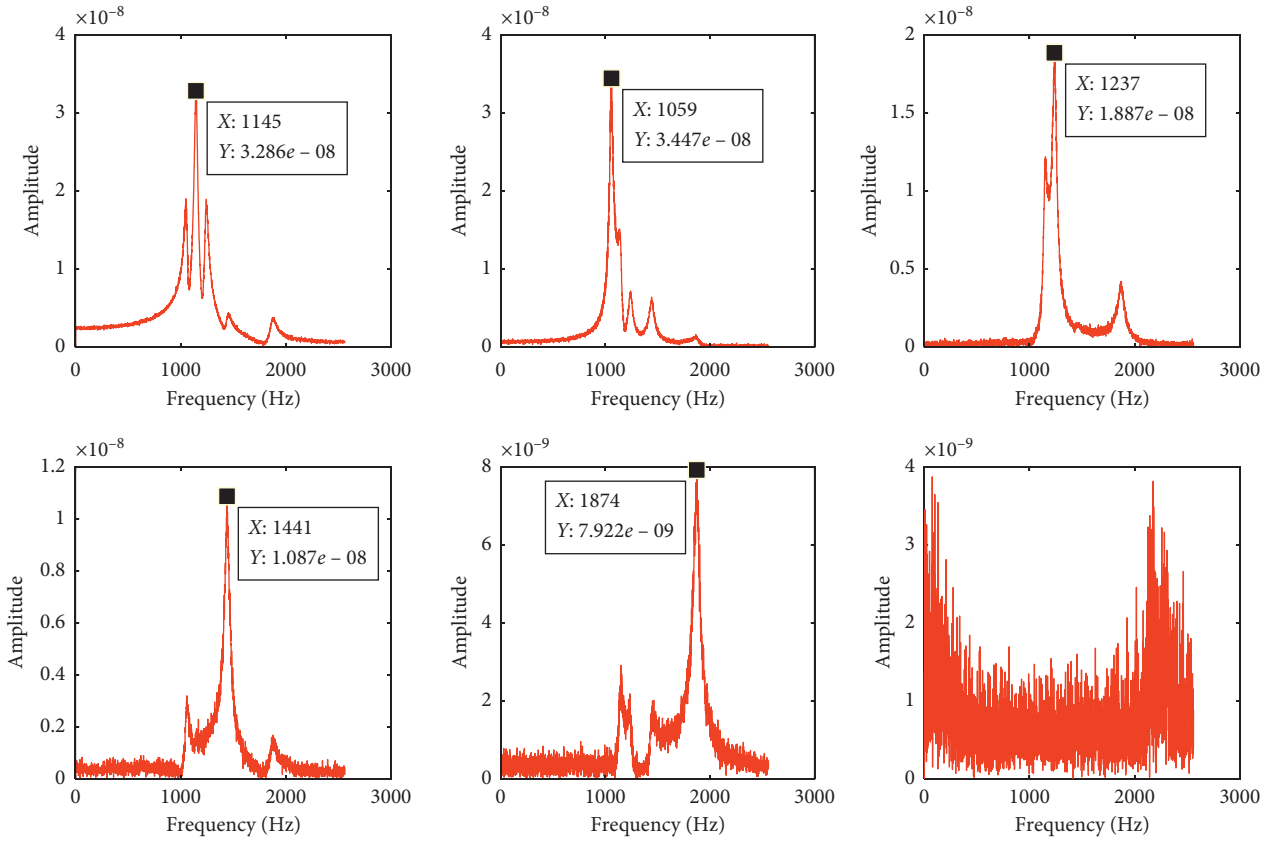

Figure 11: Modal frequencies identified by LSMS-based Isomap.

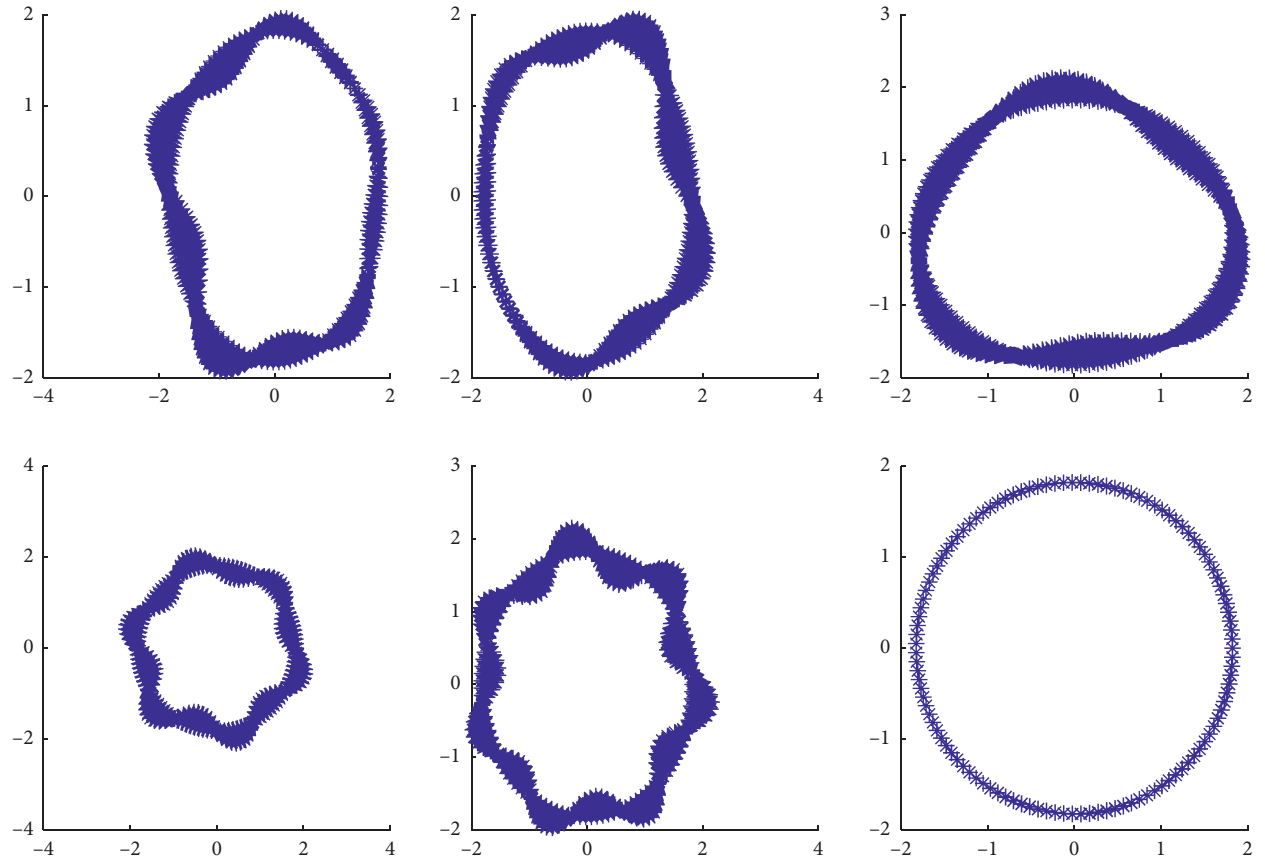

Figure 12: Modal shapes identified by DMA-based Isomap.

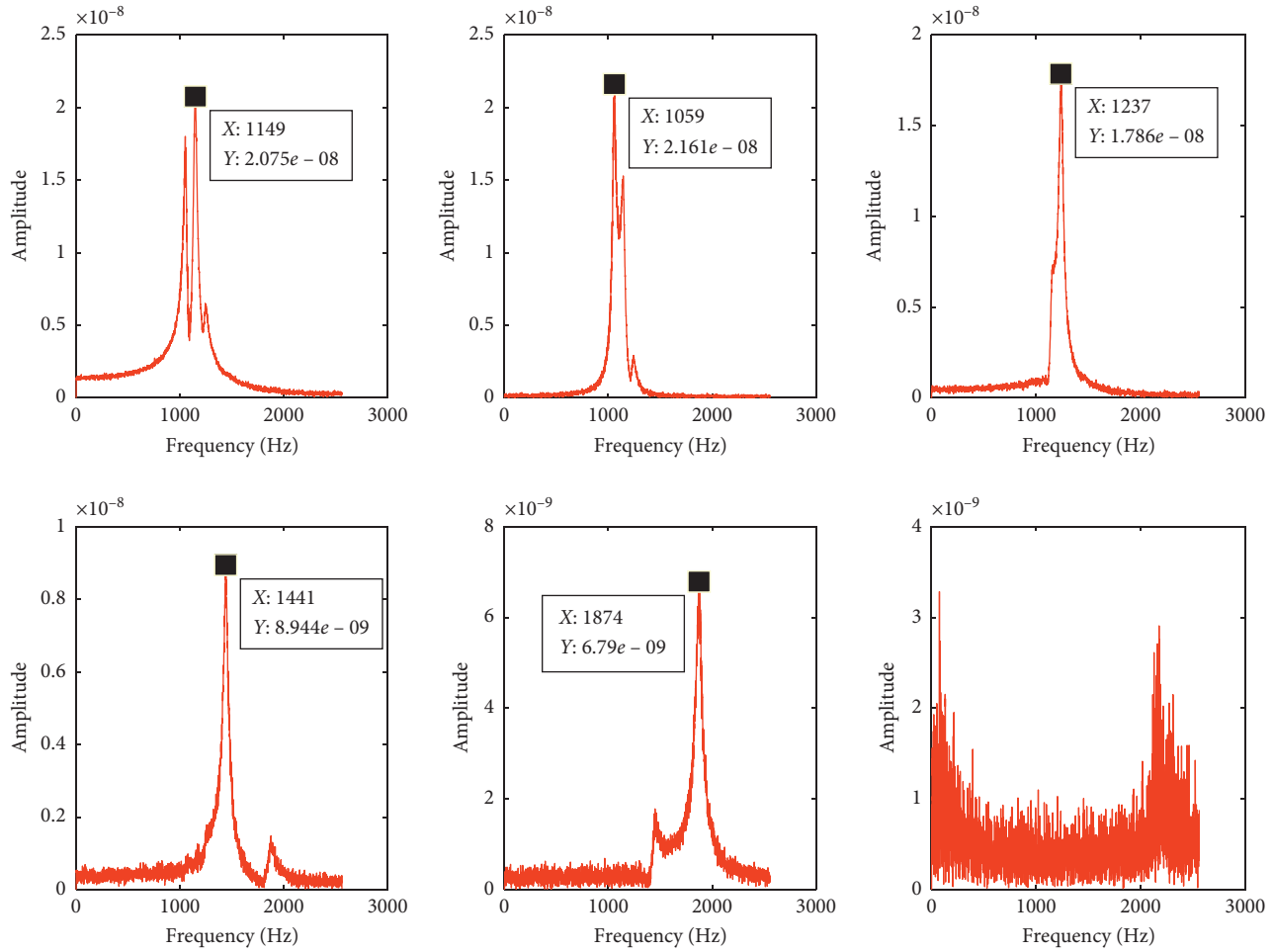

Figure 13: Modal frequencies identified by DMA-based Isomap.

Table 2: Comparison of natural frequencies with different assembly methods.

Orders	Frequency calculated by FEA (frequency/Hz)	Orders of Isomap components	Identified by LSMS-based Isomap (frequency/Hz)	Relative error (%)	Identified by DMA-based Isomap (frequency/Hz)	Relative error (%)
1	1054.9	2	1059	0.387	1059	0.387
2	1145.7	1	1145	−0.061	1149	0.288
3	1239.6	3	1237	−0.210	1237	−0.210
4	1441.9	4	1441	−0.062	1441	−0.062
5	1740.0	6	—	—	—	—
7	1871.7	5	1874	0.123	1874	0.123

The symbol "--" indicates that the result was not recognized or too small.

Table 3: Comparison of MAC of modal shapes with different assembly methods.

Order of real modal shape	Order of identified modal shape	*MAC* identified by the LSMS-based Isomap	*MAC* identified by DMA-based Isomap
1	2	0.8783	0.6564
2	1	0.6837	0.6180
3	3	0.5634	0.7817
4	4	0.4238	0.5241
5	6	0.0014	0.0049
7	5	0.6495	0.8932

Table 4: Comparison of modal shapes with different methods.

Method	Modal shapes when $K = 40$ and damping ratio is 0.03					
	1th order	2th order	3th order	4th order	5th order	7th order
FEA	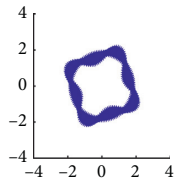	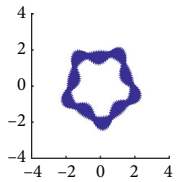	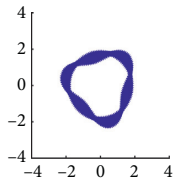	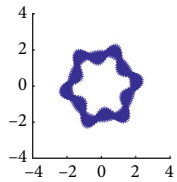	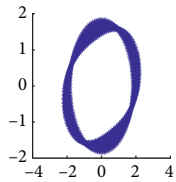	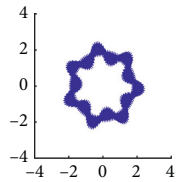
LSMS	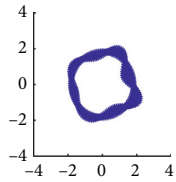	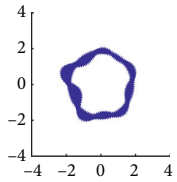	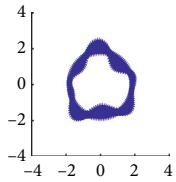	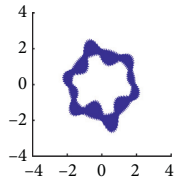	—	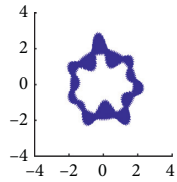
DMA	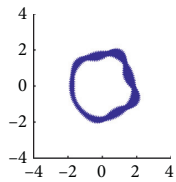	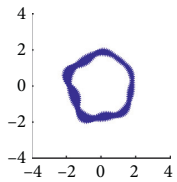	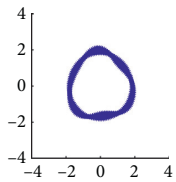	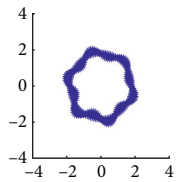	—	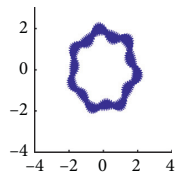

Table 5: Comparison of modal ratios with different assembly methods.

Order of real modal ratios	Order of identified modal ratios	Identified by the LSMS-based Isomap	Identified by DMA-based Isomap
1	2	0.0204	0.0286
2	1	0.0187	0.0196
3	3	0.0270	0.0210
4	4	0.0216	0.0214
5	6	—	0.0678
7	5	0.0282	0.0277

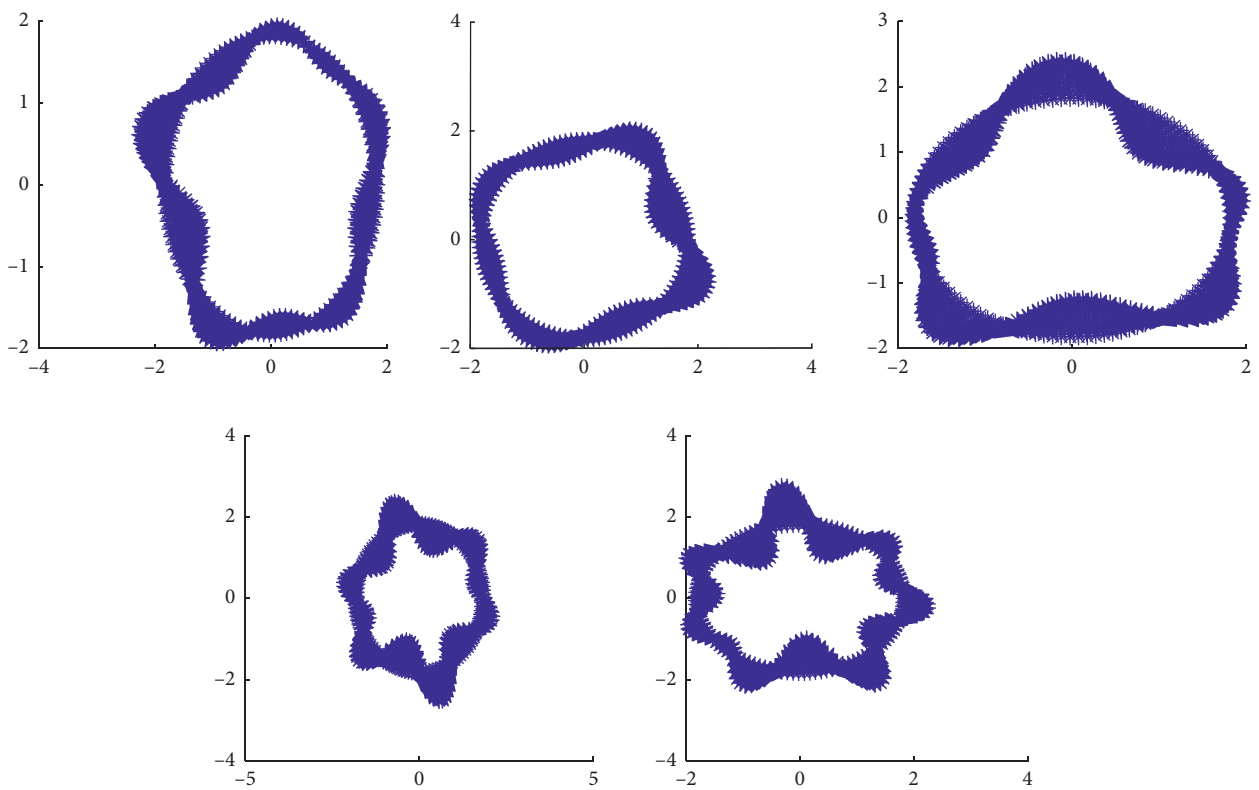

Figure 14: Modal shapes identified when the embedding dimension is 5.

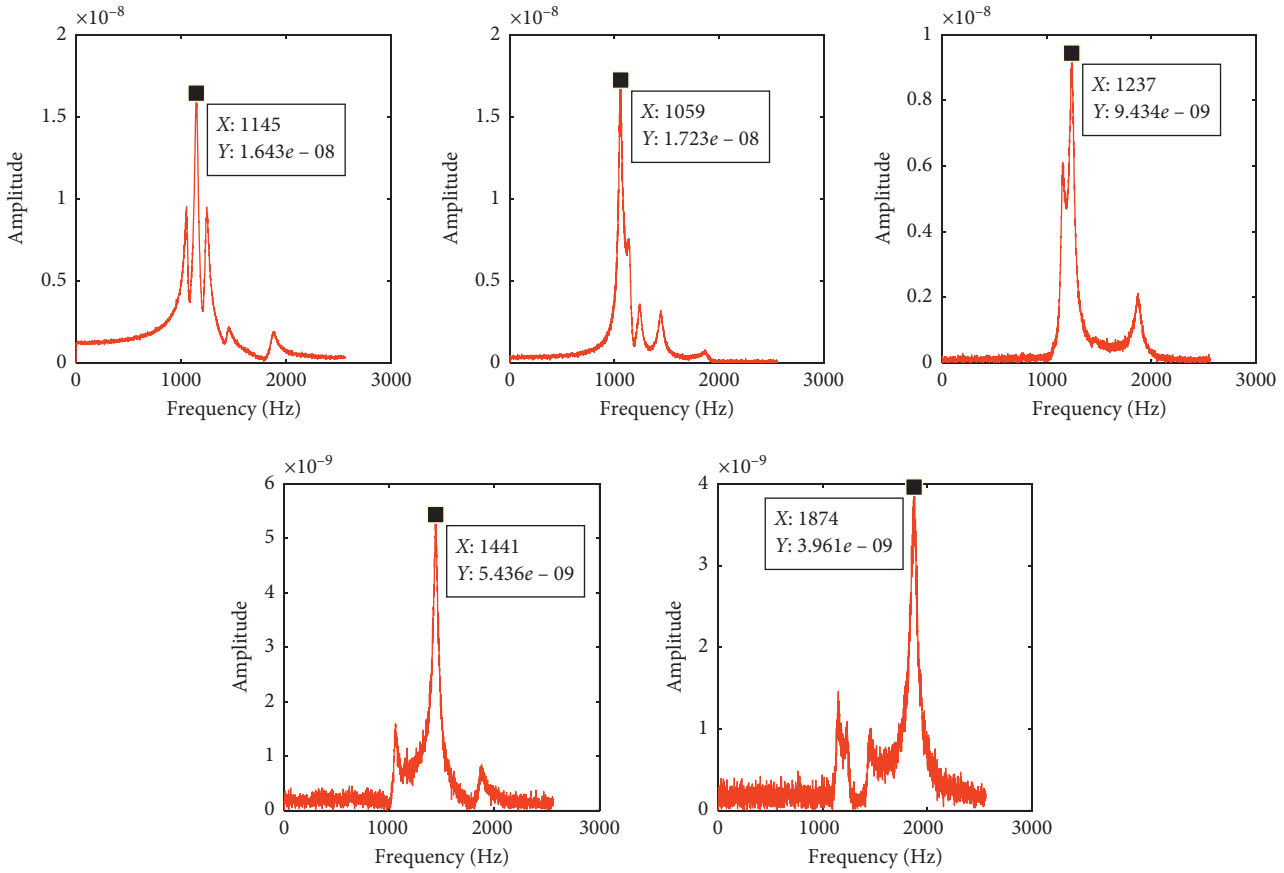

Figure 15: Modal frequencies identified when the embedding dimension is 5.

Table 6: Comparison of MAC at different dimensions.

FEA method	LSMS method			
	$d = 5$		$d = 6$	
Real order	Identify order	*MAC*	Order	*MAC*
1	2	0.8783	2	0.8783
2	1	0.6837	1	0.6837
3	3	0.5634	3	0.5634
4	4	0.4238	4	0.4238
5	6	—	6	0.0014
7	5	0.6495	5	0.6495

Table 7: Comparison of modal frequencies at different dimensions.

FEA method		LSMS method			
		$d = 5$		$d = 6$	
Real order	Real frequencies	Identify order	Frequencies	Order	Frequencies
1	1054.9	2	1059	2	1059
2	1145.7	1	1145	1	1145
3	1239.6	3	1237	3	1237
4	1441.9	4	1441	4	1441
5	1740.0	6	—	6	—
7	1871.7	5	1874	5	1874

Table 8: Comparison of MAC for different neighbor numbers K.

Real order		1	2	3	4	5	7
Identify order		2	1	3	4	6	5
$K = 12$	LSMS	0.8850	0.6863	0.5591	0.4179	0.0003	0.6544
	DMA	0.6609	0.6198	0.7790	0.5221	0.0002	0.8877
$K = 40$	LSMS	0.8783	0.6837	0.5634	0.4238	0.0014	0.6495
	DMA	0.6564	0.6180	0.7817	0.5241	0.0049	0.8932
$K = 200$	LSMS	0.8800	0.6851	0.5632	0.4261	0.0050	0.6534
	DMA	0.6599	0.6208	0.7820	0.5260	0.0042	0.8981
$K = 500$	LSMS	0.8798	0.6851	0.5635	0.4262	0.0519	0.6532
	DMA	0.6594	0.6206	0.7824	0.5263	0.0213	0.8990
$K = 800$	LSMS	0.8796	0.6851	0.5636	0.4265	0.1423	0.6543
	DMA	0.6585	0.6201	0.7827	0.5271	0.0724	0.9007

Table 9: Comparison of modal frequencies for different neighbor numbers K.

Real order		1	2	3	4	5	7
Identify order		2	1	3	4	6	5
$K = 12$	LSMS	1052	1146	1237	1441	—	1874
	DMA	1059	1145	1243	1441	—	1874
$K = 40$	LSMS	1059	1145	1237	1441	—	1874
	DMA	1059	1149	1237	1441	—	1874
$K = 200$	LSMS	1059	1145	1237	1443	—	1868
	DMA	1059	1149	1237	1443	—	1868
$K = 500$	LSMS	1059	1145	1237	1443	—	1868
	DMA	1059	1149	1237	1443	—	1868
$K = 800$	LSMS	1059	1146	1237	1443	—	1868
	DMA	1059	1149	1237	1443	—	1868
	FEA	1054.9	1145.7	1239.6	1441.9	1740.0	1871.7

Table 10: Comparison of modal ratios for different neighbor numbers K.

Real order		1	2	3	4	5	7
Identify order		2	1	3	4	6	5
$K = 12$	LSMS	0.0201	0.0186	0.0272	0.0216	0.0846	0.0294
	DMA	0.0286	0.0195	0.0211	0.0216	0.0668	0.0284
$K = 40$	LSMS	0.0204	0.0187	0.0270	0.0216	0.1140	0.0282
	DMA	0.0286	0.0196	0.0210	0.0214	0.0678	0.0277
$K = 200$	LSMS	0.0204	0.0187	0.0270	0.0213	0.0702	0.0275
	DMA	0.0285	0.0196	0.0210	0.0212	0.0317	0.0275
$K = 500$	LSMS	0.0204	0.0187	0.0271	0.0212	0.0560	0.0274
	DMA	0.0285	0.0196	0.0210	0.0211	0.0364	0.0274
$K = 800$	LSMS	0.0204	0.0188	0.0271	0.0212	0.0592	0.0274
	DMA	0.0286	0.0196	0.0210	0.0211	0.0359	0.0274

dimensional case. Therefore, in Isomap, the selected dimension has no effect on the identification of the modal parameters of the first few orders.

(4) Different K values have little effect on the recognition results (see Tables 8–10). As K increases, the identification accuracy of later orders increases. However, the time complexity of the algorithm also increases.

(5) Tables 11–13 indicate that the modal ratios can be effectively identified using both RDT and NExT. The different dimensionality reduction methods (PCA or MDS and Isomap) and assembly methods (LSMS and DMA) have little impact on the estimated modal ratios.

(6) Isomap-based OMA can effectively identify the three-dimensional modal parameters (see Tables 11–16). The 6th-order modal parameters are not extracted well by Isomap because of their weak nonlinear characteristics.

(7) Tables 11–19 illustrate that, as the real modal ratio increases, the modal shapes, frequencies, and modal ratios become more difficult to identify. This is because a larger damping ratio results in smaller structure responses.

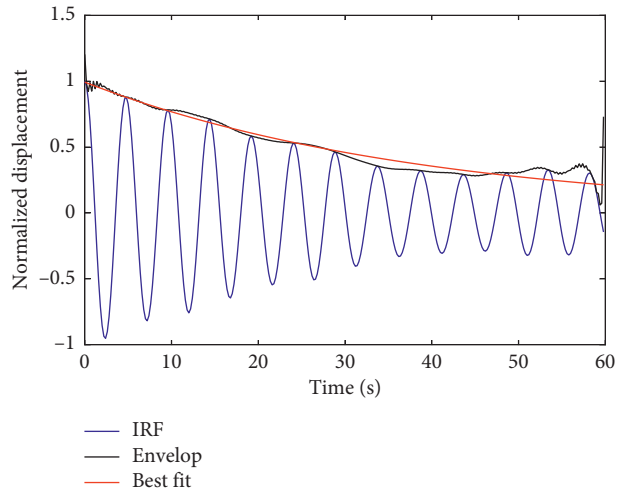

Figure 16: Example of the modal ratio solution process.

Table 11: RDT and NExT results with a real modal damping ratio of 0.1.

Real order	Identified order	Real modal ratio = 0.1							
		PCA (MDS)				Isomap			
		LSMS		DMA		LSMS		DMA	
		RDT	NExT	RDT	NExT	RDT	NExT	RDT	NExT
1	2	0.0532	0.0567	0.0587	0.0624	0.0510	0.0567	0.0605	0.0627
2	1	0.1155	0.1241	0.1045	0.1139	0.1136	0.1245	0.1074	0.1139
3	3	0.0668	0.0639	0.0650	0.0605	0.0682	0.0645	0.0653	0.0612
4	4	0.0716	0.0847	0.0869	0.0967	0.0770	0.0837	0.0956	0.0971
5	6	0.0742	0.0758	0.0748	0.0759	—	—	—	—
7	5	0.1079	0.1192	0.1308	0.1351	0.1369	0.1388	0.1473	0.1420

Table 12: RDT and NExT results with a real modal damping ratio of 0.05.

Real order	Identified order	Real modal ratio = 0.05							
		PCA (MDS)				Isomap			
		LSMS		DMA		LSMS		DMA	
		RDT	NExT	RDT	NExT	RDT	NExT	RDT	NExT
1	2	0.0312	0.0331	0.0312	0.0454	0.0297	0.0331	0.0373	0.0442
2	1	0.0716	0.0854	0.0585	0.0679	0.0825	0.0861	0.0549	0.0673
3	3	0.0388	0.0410	0.0543	0.0611	0.0391	0.0410	0.0524	0.0597
4	4	0.0274	0.0367	0.0625	0.0780	0.0298	0.0368	0.0619	0.0821
5	6	0.0434	0.0450	0.0361	0.0450	—	—	0.0364	0.0471
7	5	0.0492	0.0485	0.0393	0.0453	0.0499	0.0496	0.0416	0.0462

Table 13: RDT and NExT results with a real modal damping ratio of 0.03.

Real order	Identified order	Real modal ratio = 0.03							
		PCA (MDS)				Isomap			
		LSMS		DMA		LSMS		DMA	
		RDT	NExT	RDT	NExT	RDT	NExT	RDT	NExT
1	2	0.0185	0.0204	0.0213	0.0286	0.0181	0.0204	0.0206	0.0286
2	1	0.0183	0.0188	0.0160	0.0197	0.0167	0.0187	0.0163	0.0196
3	3	0.0230	0.0271	0.0212	0.0209	0.0230	0.0270	0.0212	0.0210
4	4	0.0168	0.0212	0.0149	0.0210	0.0160	0.0216	0.0163	0.0214
5	6	0.0270	0.0267	0.0269	0.0267	—	—	0.0550	0.0678
7	5	0.0275	0.0274	0.0290	0.0274	0.0298	0.0282	0.0297	0.0277

Table 14: PCA and Isomap by LSMS with a real modal damping ratio of 0.03.

		LSMS					
Real order	Identified order	PCA (MDS)			Isomap		
		MAC	Frequencies	Relative error (%)	MAC	Frequencies	Relative error (%)
1	2	0.8785	1058	0.294	0.8783	1059	0.389
2	1	0.6843	1145	−0.061	0.6837	1145	−0.061
3	3	0.5639	1237	−0.210	0.5634	1237	−0.210
4	4	0.4274	1442	0.007	0.4238	1441	−0.062
5	6	0.6282	1737	−0.172	0.0014	—	—
7	5	0.6564	1872	0.016	0.6495	1874	0.123

Table 15: PCA and Isomap by LSMS with a real modal damping ratio of 0.05.

		LSMS					
Real order	Identified order	PCA (MDS)			Isomap		
		MAC	Frequencies	Relative error (%)	MAC	Frequencies	Relative error (%)
1	2	0.6311	1059	0.389	0.6316	1065	0.957
2	1	0.3026	1143	−0.236	0.3019	1143	−0.236
3	3	0.1082	1232	−0.613	0.1088	1229	−0.855
4	4	0.0801	1437	−0.340	0.0788	1441	−0.062
5	6	0.0037	1747	0.402	0.0227	—	—
7	5	0.0219	1868	−0.198	0.0211	1879	0.390

Table 16: PCA and Isomap by LSMS with a real modal damping ratio of 0.1.

		LSMS					
Real order	Identified order	PCA (MDS)			Isomap		
		MAC	Frequencies	Relative error (%)	MAC	Frequencies	Relative error (%)
1	2	0.7248	1073	1.716	0.7256	1080	2.379
2	1	0.4890	1140	−0.498	0.4887	1137	−0.759
3	3	0.3430	1199	−3.275	0.3379	1178	−4.969
4	4	0.2435	1414	−1.935	0.2434	1391	−3.530
5	6	0.6293	1747	0.402	0.0002	—	—
7	5	0.2520	1854	−0.946	0.2710	1800	−3.831

Table 17: PCA and Isomap by DMA with a real modal damping ratio of 0.03.

		DMA					
Real order	Identified order	PCA (MDS)			Isomap		
		MAC	Frequencies	Relative error (%)	MAC	Frequencies	Relative error (%)
1	2	0.6554	1059	0.389	0.6564	1059	0.389
2	1	0.6180	1151	0.463	0.6180	1149	0.288
3	3	0.7833	1237	−0.210	0.7817	1237	−0.210
4	4	0.5284	1443	0.076	0.5241	1441	−0.062
5	6	0.7289	1738	−0.115	0.0049	—	—
7	5	0.9038	1873	0.069	0.8932	1874	0.123

Table 18: PCA and Isomap by DMA with a real modal damping ratio of 0.05.

		DMA					
Real order	Identified order	PCA (MDS)			Isomap		
		MAC	Frequencies	Relative error (%)	MAC	Frequencies	Relative error (%)
1	2	0.5395	1052	−0.275	0.5614	1052	−0.275
2	1	0.1402	1143	−0.236	0.1521	1140	−0.498
3	3	0.1928	1225	−1.178	0.1770	1237	−0.210
4	4	0.1213	1434	−0.548	0.1245	1441	−0.062
5	6	0.0005	1877	7.874	0.0003	1889	8.563
7	5	0.0041	1879	0.390	0.0044	1890	0.978

Table 19: PCA and Isomap by DMA with a real modal damping ratio of 0.1.

Real order	Identified order	DMA					
		PCA (MDS)			Isomap		
		MAC	Frequencies	Relative error (%)	MAC	Frequencies	Relative error (%)
1	2	0.5232	1081	1.716	0.5193	1081	2.474
2	1	0.4812	1044	−0.498	0.4804	1138	−0.672
3	3	0.2107	1185	−4.405	0.2033	1176	−5.131
4	4	0.1703	1406	−2.490	0.1788	1392	−3.461
5	6	0.7279	1747	0.402	0.0003	—	—
7	5	0.4739	1854	−0.946	0.5082	1889	0.924

5. Conclusion and Prospects

In this paper, we have described the application of the Isomap algorithm to OMA to identify modal shapes, modal natural frequencies, and modal ratios of three-dimensional structures. Promising results were obtained from simulations of a cylindrical shell emitting nonlinear response patterns. We also compared the influence of various parameters. The simulation results show that the parameters of the Isomap algorithm (number of neighbors K and dimension d) have little effect on the results. However, the structural parameters (damping ratio) and matrix assembly method have a significant influence on the output. Furthermore, we compared the results of PCA (MDS) with Isomap.

In future work, we will attempt to improve the accuracy of our method at higher damping ratios. The method discussed in this paper uses the most basic Isomap algorithm. Improved versions of Isomap may achieve better results. Furthermore, the experiment with the actual structure and the problem of finding the missing mode are worth studying.

Data Availability

All the data used to support the findings of this study are available from the corresponding author upon request.

Conflicts of Interest

The authors declare that there are no conflicts of interest regarding the publication of this paper.

Acknowledgments

This work was financially supported by the National Natural Science Foundation of China (Grant no. 51305142) and the Promotion Program for Young and Middle-Aged Teachers in Science and Technology Research at Huaqiao University under Grant ZQN-PY212.

References

[1] M. Ghalishooyan and M. Abdelghani, "Output-only damping estimation of structures using enhanced frequency domain decomposition method," *Modares Civil Engineering Journal*, vol. 18, no. 2, pp. 183–193, 2018.

[2] H.-F. Lam, J. Hu, and J.-H. Yang, "Bayesian operational modal analysis and Markov chain Monte Carlo-based model updating of a factory building," *Engineering Structures*, vol. 132, pp. 314–336, 2017.

[3] G. P. Martindale, "Structural identification and assessment of the inverted tee girder bridge system," MS thesis, University of Nebraska-Lincoln, Lincoln, NE, USA, 2018.

[4] H. Zhou, K. Yu, Y. Chen, R. Zhao, and Y. Wu, "Output-only modal estimation using sparse component analysis and density-based clustering algorithm," *Measurement*, vol. 126, pp. 120–133, 2018.

[5] K. Yu, K. Yang, and Y. Bai, "Estimation of modal parameters using the sparse component analysis based underdetermined blind source separation," *Mechanical Systems and Signal Processing*, vol. 45, no. 2, pp. 302–316, 2014.

[6] J. Wang, C. Wang, T. Zhang, and B. Zhong, "Comparison of different independent component analysis algorithms for output-only modal analysis," *Shock and Vibration*, vol. 2016, Article ID 6309084, 25 pages, 2016.

[7] W. K. Härdle and Z. Hlávka, "Principal component analysis," *IEEE Transactions on Automatic Control*, vol. 29, no. 1, pp. 163–183, 2015.

[8] X. Li, C. Cai, and J. He, "Density-based multi-manifold ISOMAP for data classification," in *Proceedings of the Asia-Pacific Signal and Information Processing Association Annual Summit and Conference (APSIPA ASC)*, pp. 897–903, IEEE, Kuala Lumpur, Malaysia, December 2017.

[9] X. He, S. Yan, Y. Hu et al., "Face recognition using laplacianfaces," *IEEE Transactions on Pattern Analysis and Machine Intelligence*, vol. 27, no. 3, pp. 328–340, 2005.

[10] S. Bai, X. Bai, L. J. Latecki et al., "Multidimensional scaling on multiple input distance matrices," *AAAI*, pp. 1281–1287, 2017.

[11] A. J. Izenman, "Linear discriminant analysis," in *Modern Multivariate Statistical Techniques*, pp. 237–280, Springer, New York, NY, USA, 2013.

[12] C. Wang, J. Gou, J. Bai et al., "Modal parameter identification with principal component analysis," *Journal of Xi'an Jiaotong University*, vol. 47, no. 11, pp. 97–104, 2013.

[13] C. Wang, W. Guan, J. Gou et al., "Principal component analysis based three-dimensional operational modal analysis," *International Journal of Applied Electromagnetics and Mechanics*, vol. 45, no. 1–4, pp. 137–144, 2014.

[14] C. Wang, J. Wang, and Y. Zhang, "Operational modal analysis of three-dimensional structures by second-order blind identification and least square generalized inverse," *Journal of Vibroengineering*, vol. 19, no. 4, pp. 2857–2872, 2017.

[15] J. P. Noël and G. Kerschen, "Nonlinear system identification in structural dynamics: 10 more years of progress," *Mechanical Systems and Signal Processing*, vol. 83, pp. 2–35, 2016.

[16] S. T. Roweis and L. K. Saul, "Nonlinear dimensionality reduction by locally linear embedding," *Science*, vol. 290, no. 5500, pp. 2323–2326, 2000.

[17] C. Sun, P. Wang, R. Yan, R. X. Gao, and X. Chen, "Machine health monitoring based on locally linear embedding with kernel sparse representation for neighborhood optimization,"

Mechanical Systems and Signal Processing, vol. 114, pp. 25–34, 2019.

[18] M. Belkin and P. Niyogi, "Laplacian eigenmaps for dimensionality reduction and data representation," *Neural Computation*, vol. 15, no. 6, pp. 1373–1396, 2003.

[19] S. W. Choi, C. Lee, J.-M. Lee, J. H. Park, and I.-B. Lee, "Fault detection and identification of nonlinear processes based on kernel PCA," *Chemometrics and Intelligent Laboratory Systems*, vol. 75, no. 1, pp. 55–67, 2005.

[20] S. K. Prabhakar and H. Rajaguru, "Comparison of Isomap and matrix factorization with mahalanobis based sparse representation classifier for epilepsy classification from EEG signals," in *Proceedings of the 2017 IEEE Region 10 Humanitarian Technology Conference (R10-HTC)*, pp. 580–583, IEEE, Dhaka, Bangladesh, December 2017.

[21] J. Bai, G. Yan, and C. Wang, "Modal identification method following locally linear embedding," *Journal of Xi'an Jiaotong University*, vol. 47, no. 1, 2013.

[22] J. Zhang, L. Dong, Y. Guirong et al., "Improved LLE algorithm and its application," *International Journal of Applied Electromagnetics and Mechanics*, vol. 52, no. 1-2, pp. 685–690, 2016.

[23] L. Dong, C. Hao, and J. Zhang, "Modal identification and influence factors of LLE algorithm," *Structure & Environment Engineering*, vol. 44, no. 05, pp. 41–46, 2017.

[24] W. Guan, J. M. Dong, Y. Han, and J. Zhou, "Data-driven methods for operational modal parameters identification: a comparison and application," *Measurement*, vol. 132, pp. 238–251, 2019.

[25] J. B. Tenenbaum, V. De Silva, and J. C. Langford, "A global geometric framework for nonlinear dimensionality reduction," *Science*, vol. 290, no. 5500, pp. 2319–2323, 2000.

[26] K.-K. Xu, H.-X. Li, and Z. Liu, "ISOMAP-based spatiotemporal modeling for lithium-ion battery thermal process," *IEEE Transactions on Industrial Informatics*, vol. 14, no. 2, pp. 569–577, 2018.

[27] M. Balasubramanian and E. L. Schwartz, "The isomap algorithm and topological stability," *Science*, vol. 295, no. 5552, pp. 7a–7, 2002.

[28] T. Zhang, C. Wang, and Y. Zhang, "Three-dimensional operational modal analysis based on self-iteration principal component extraction and direct matrix assembly," *Journal of Vibroengineering*, vol. 19, no. 8, 2017.

[29] K. A. Basov, "ANSYS and LMS virtual Lab," *Geometric Modeling*, p. 240, 2006.

[30] S. R. Ibrahim, "Random decrement technique for modal identification of structures," *Journal of Spacecraft and Rockets*, vol. 14, no. 11, pp. 696–700, 1977.

[31] G. H. James, T. G. Carne, and J. P. Lauffer, "The natural excitation technique (NExT) for modal parameter extraction from operating structures," *Modal Analysis-The International Journal of Analytical and Experimental Modal Analysis*, vol. 10, no. 4, p. 260, 1995.